coatings

MDPI

Article

Preparation and Performance Study of Sand-Containing Hollow Concrete with Alkali-Activated Recycled Concrete Powder Based on Target Porosity

Yuanxin Guo [1], Wenna Li [1], Zhizhu Zhang [1,*], Gongbing Yue [1], Xingang Xu [2], Qiuyi Li [1,*], Changhai Shao [3] and Mingxu Chen [1]

[1] College of Civil Engineering & Architecture, Qingdao Agricultural University, Qingdao 266109, China; 201901012@qau.edu.cn (Y.G.); 20252113006@stu.qau.edu.cn (W.L.)
[2] State Key Laboratory of Silicate Materials for Architectures, Wuhan University of Technology, Wuhan 430070, China
[3] Shandong Guanrunjia Environmental Protection New Materials Co., Ltd., Zibo 255000, China
* Correspondence: 20232113006@stu.qau.edu.cn (Z.Z.); 201801001@qau.edu.cn (Q.L.)

Highlights

What are the main findings?

- Recycled powder activity indices at various grinding times were compared. Calculated and theoretical porosities of al-kali-activated sand-containing macroporous concrete were quantified.
- Image binarization uncovered the porosity deviation mechanism. Binder content and pore volume govern concrete me-chanical and permeability properties.

What are the implications of the main findings?

- Verified porosity calculation supports mix design optimization of alkali-activated porous concrete.
- Mechanical-permeability regulation enables precise performance design for engineering applications.

Abstract

With the aim of reducing greenhouse gas emissions from energy consumption and advancing the green energy transition, this study employs sodium hydroxide and water glass as activators to facilitate the replacement of fossil fuels with renewable energy sources, with physically activated recycled micro-powder serving as an auxiliary cementitious material to prepare alkali-activated recycled hollow concrete. This study pioneers the application of the coarse aggregate tight-packing theory (bulk density method) to the preparation of alkali-activated recycled hollow concrete containing sand. By integrating Matlab image binarization techniques, we quantitatively analyzed the causes of porosity deviation, achieving precise alignment between target and actual porosity. This work fills a theoretical gap in the quantitative design of porosity for this concrete type. Additionally, the effects of different binder material dosages and pore volumes on the mechanical properties and permeability coefficients of sand-containing porous concrete were evaluated. Experimental results indicate that the calculated pore volume of sand-containing porous concrete prepared using the dense-packing theory (bulk density method) exhibits a smaller average error compared to the actual pore volume. As the amount of cementitious materials increases, the compression strength of permeable concrete gradually increases. When the cementitious material content is 450 kg/m^3, and the target porosity is 15%, the concrete's

Check for updates

Academic Editor: Paolo Castaldo

Received: 8 February 2026
Revised: 23 February 2026
Accepted: 28 February 2026
Published: 4 March 2026
Corrected: 11 May 2026

Copyright: © 2026 by the authors. Licensee MDPI, Basel, Switzerland. This article is an open access article distributed under the terms and conditions of the Creative Commons Attribution (CC BY) license.

28-day compressive strength reaches 21.4 MPa. At a porosity of 15%, the permeability coefficient ranges from 5.2 to 5.7 mm/s.

Keywords: recycled micro powder; close packing theory; close wrapping theory; porosity; alkali activation

1. Introduction

With the ongoing advancement of global urbanization, by 2025, the annual production of solid waste generated throughout the entire lifecycle of buildings is expected to reach approximately four billion tons, but the average resource utilization rate is only about 30% to 40%; approximately 80% of construction waste can be converted into building materials such as recycled aggregates and recycled micro-powders after undergoing processes like crushing and activation. The resource utilization rate of industrial solid waste (including slag, steel slag, fly ash, etc.) can exceed 80%. Among municipal solid waste, only the lightweight aggregate components (approximately 30%) that undergo harmless treatment can be utilized for building materials. A large amount of untreated construction waste is disposed of through crude landfilling, which not only exacerbates pressure on land resources but also causes multiple environmental risks due to dust dispersion [1–4]. Recycled concrete aggregate (RCA) is an alternative material produced by processing waste concrete into natural aggregate (NA) and has become one of the primary sustainable methods for disposing of construction demolition waste. This technology not only effectively alleviates the issue of insufficient landfill capacity but also reduces excessive extraction of natural aggregate resources. Recycled concrete powder (RCP), generated during the RCA recycling process, is characterized by fine particles smaller than 150 μm. In recent years, the application of recycled aggregates and mineral admixtures in the construction field has increasingly attracted attention from both the academic and engineering communities. These materials not only effectively alleviate the pressure of solid waste disposal and reduce environmental pollution risks but also significantly reduce construction costs [5,6]. As a sustainable alternative to natural aggregates, it is a promising method for minimizing construction waste. However, RCA recovered from the CDW surface is covered with a thick layer of old mortar, and its porous pores and micro-cracks can hinder the hydration reaction to some extent, thereby reducing the performance of the specimens [7–9].

Research indicates that recycled coarse aggregate (RCA) generally exhibits lower particle density than natural coarse aggregate (NCA), while its crushing index and water absorption rate are significantly higher than those of NCA. Bacus et al. prepared permeable concrete using RCA replacing 40%, 50%, and 60% of NCA, achieving a 10% increase in permeability coefficient at a 50% replacement rate [10]. Ma et al. discovered that carbonating recycled aggregates with CO_2 enhances the splitting tensile strength of permeable concrete, with the maximum increase reaching 100% [11]. Some researchers improved recycled aggregate properties by incorporating geopolymers, such as pre-treating RCA with fly ash-based geopolymer (FGP) to form a reinforcing layer and generate C(N)-A-S-H gel [12–14]. However, its overall performance remains inferior to that of concrete using natural aggregates.

The type and dosage of cementitious materials significantly influence concrete workability and mechanical properties. Appropriate material selection is crucial for enhancing the performance of recycled aggregate concrete (RAC) and reducing environmental impacts. Abba et al. prepared RAC using natural pozzolan (NP), limestone powder (LP), and granulated blast furnace slag (GGBS) at varying replacement rates, confirming that supplementary cementitious materials enhance concrete performance through pore filling

and nucleation reactions [15]. Yao et al. prepared alkali-activated foam concrete using recycled concrete powder (RCP) and GGBS. The gel produced during hydration partially filled pores, enhancing density [16].

Permeable concrete exhibits excellent permeability due to its absence or low content of sand, combining slope protection and ecological exchange functions. It is widely applied in sponge city construction, such as parking lots and urban road surfaces [8,17–19]. Traditional permeable concrete uses cement as a binder, resulting in low hardened strength and high energy consumption and carbon emissions during production. Consequently, researchers are exploring alkali-activated binders to enhance their mechanical properties [20–22]. Li et al. reported that co-blending silica fume and steel fibers in RAC enhances toughness and tensile strength, while silica fume reduces porosity through a "micro-aggregate filling effect" [23]. Tan et al. investigated the effect of basalt fibers on the mechanical properties of fly ash–slag geopolymer permeable concrete. They found that fiber length should be less than 12 mm and volume fraction should not exceed 0.15% to prevent clogging of interconnected pores [24]. Zheng et al. incorporated copper slag (CS) into alkali-activated permeable concrete and observed that both porosity and permeability increased with higher CS content [25].

Recycled cement powder (RCP), a byproduct of RCA recycling with a composition similar to fly ash, has been studied as a cement substitute to reduce carbon footprint. However, directly obtained RCP exhibits high porosity and low hydration activity [26], requiring pretreatment such as calcination, grinding, or carbonization for effective utilization [27–29]. Advancing sustainability necessitates addressing the core environmental challenges of conventional methods—namely, the high energy consumption of calcination and the substantial carbon emissions associated with carbonization. This study enhances the reactivity index of RCP through mechanical grinding. Using granulated blast furnace slag powder (GGBS), fly ash (FA), and the activated RCP as cementitious materials, alkali-activated sand-containing recycled hollow concrete (AASCRHC) was prepared. Two theories (compact packing theory and compact filling theory) were employed to prepare sand-containing hollow concrete with varying porosities (15%, 20%, 25%). The deviation between the target porosity and the actual porosity of the sand-containing hollow concrete was evaluated. Using Matlab R2024b, concrete sections underwent binarization processing to analyze and investigate the impact of the "edge wall effect" on sand-containing hollow concrete. Additionally, this study analyzed the effects of varying cementitious material content and porosity on the compressive strength, permeability coefficient, and freeze–thaw resistance of sand-containing AASCRHC. This research aims to enhance the utilization potential of RCP in AASCRHC and provides scientific rationale and decision support for reducing porosity deviation in sand-containing AASCRHC. The detailed research process is illustrated in Figure 1.

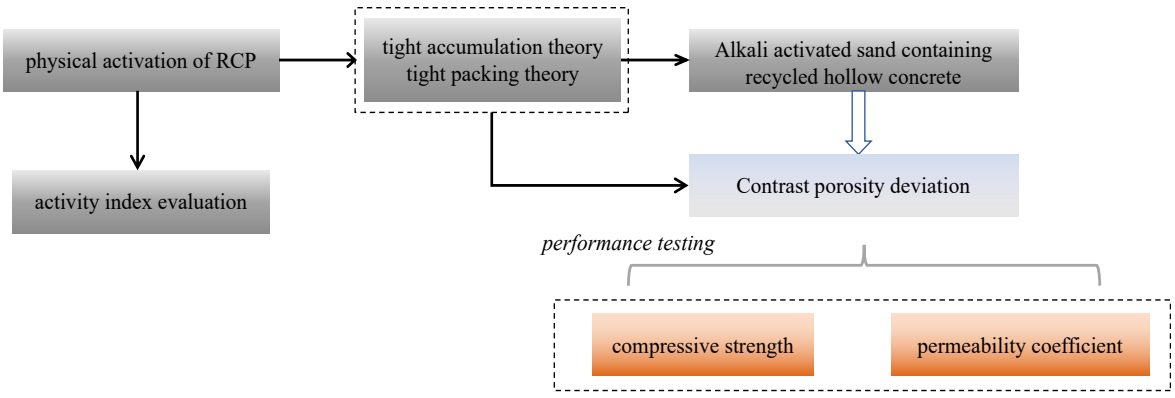

Figure 1. Research process.

2. Experimental Design

2.1. Materials

2.1.1. Binding Materials

This research utilized fly ash (FA), ground-granulated blast furnace slag (GGBS), and recycled concrete powder (RCP) as the key cementitious components. The FA and GGBS were procured from Shandong Junhong Environmental Protection Technology Co., Ltd., Zibo, Shandong Province, China and the RCP was sourced from Qingdao Green Sail Recycling Resources Co., Ltd. Qingdao, Shandong Province, China. Their fundamental physical properties were determined: FA presented a bulk density of 2370 kg/m^3 and a specific surface area of 373 m^2/kg; GGBS demonstrated values of 2860 kg/m^3 and 435 m^2/kg, respectively; for RCP, the corresponding measurements were 2600 kg/m^3 and 381.9 m^2/kg, and it also possessed a 28-day activity index of 62.7%. The elemental compositions of these materials are provided in Table 1, with their respective crystalline structures and micro-morphologies displayed in Figure 2. Pertinent characteristics of the RCP are further outlined in Table 2. Throughout the experimental phase, the alkali modulus and the alkali equivalent were held constant at 1.0 and 3.5%, respectively.

Table 1. Chemical composition of FA, GGBS, and RCP (mass fraction, %).

Material	SiO_2	Al_2O_3	CaO	Fe_2O_3	Na_2O	MgO	Other
GGBS	25.9	13.0	51.5	0.3	0.4	4.1	4.8
FA	44.3	28.6	8.6	9.1	0.8	0.6	7.9
RCP	59.6	17.4	5.8	4.9	3.1	2.4	6.8

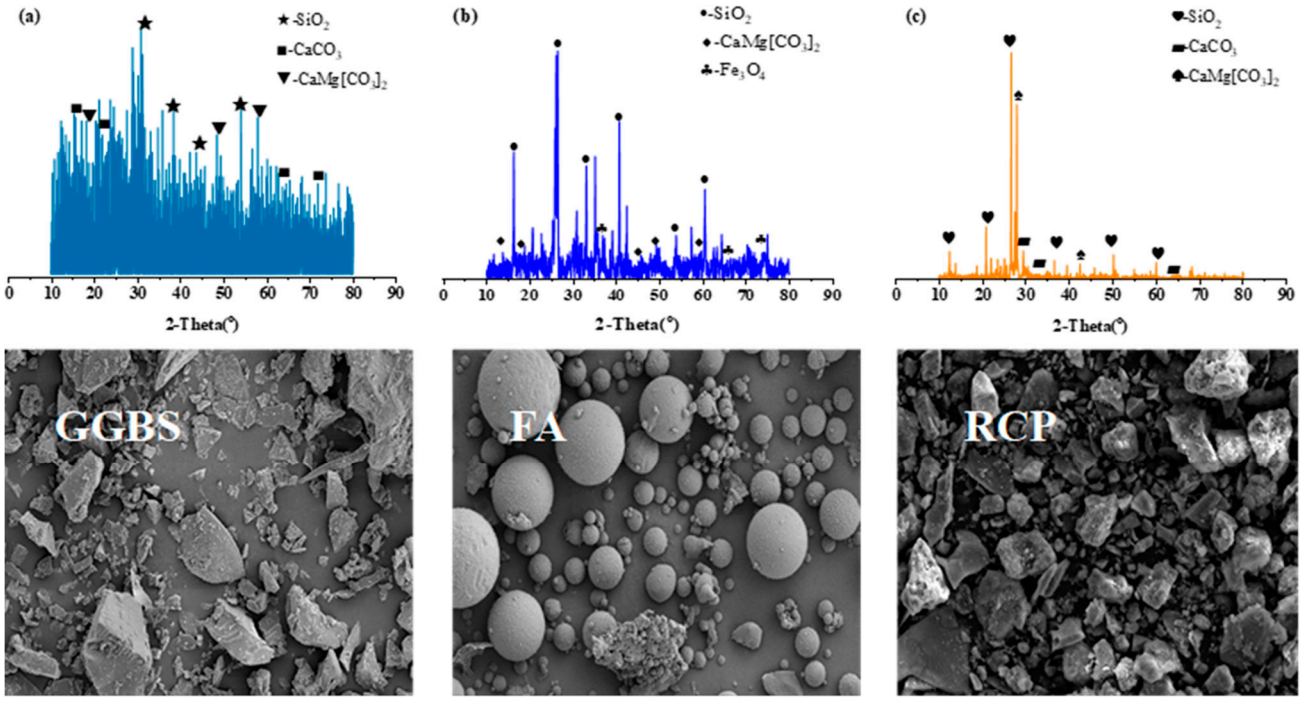

Figure 2. XRD and SEM of (**a**) GGBS, (**b**) FA, and (**c**) RCP.

Table 2. RCP performance indicators.

Material	Fluidity (mm)	2 h Fluidity Change (mm)	Water Demand Ratio (%)	Activity Index (%)
RCP	212	29.8	118	62.7

2.1.2. Recycled Aggregates

The test used Type II recycled coarse aggregates with a particle size range from 4.75 mm to 16 mm, as well as Type II recycled fine aggregates. Within this range, the mortar can effectively coat all aggregates. If the aggregate particle size is too large, the prepared mortar may not be able to fully cover all the aggregates. The specific RCA and RFA properties are shown in Table 3.

Table 3. Physical and mechanical performance characteristics of recycled aggregates.

Materials	Particle Size (mm)	Apparent Density (kg/m^3)	Bulk Density (%)	Water Absorption Rate (%)
RCA	5–16	2590	14.5	4.62
RFA	<4.75	2408	13.4	2.32

2.2. Mix Design

Given that the aggregate systems used in this study are all recycled aggregates and that recycled concrete powder (RCP) is used as the main cementitious component, this composite system exhibits significantly high water absorption characteristics. Based on the aforementioned material properties, this study prepared alkali-activated sand-containing porous concrete by adjusting key parameters such as sand content and water-to-binder ratio to achieve gradient control of porosity. During the experimental process, it was found that due to the dynamic water absorption effect of the recycled aggregate–RCP system, the water content must be dynamically adjusted in conjunction with changes in sand content and the workability of the mixture to ensure that the fresh concrete meets the requirements for forming an open-pore structure.

2.2.1. "Coarse Aggregate Tight Accumulation Theory"

This theory assumes that the apparent volume of 1 m^3 of hollow concrete is formed by the compacted filling of coarse aggregates, with the remaining mixing materials partially filling the pores according to their respective absolute volumes [30].

The mix ratio formula is shown in Formula (1):

$$\frac{m_g}{\gamma_g} + \frac{m_{ggbs}}{\gamma_{ggbs}} + \frac{m_f}{\gamma_f} + \frac{m_r}{\gamma_r} + \frac{m_w}{\gamma_w} + \frac{m_s}{\gamma_s} + p = 1 \quad (1)$$

In the above formula, m_g, m_s, $mggb_s$, m_f, m_w, and m_r represent the mass of coarse aggregate, fine aggregate, GGBS, FA, alkali solution, and RCP in 1 m^3 of concrete, respectively, with units of (kg). γ_g, γ_s, γ_{ggbs}, γ_f, γ_w, and γ_r represent the apparent density of coarse aggregate, fine aggregate, GGBS, FA, alkali solution, and RCP, respectively, with units of (kg/m^3). p denotes the connected porosity in sand-containing large-pore concrete, with units of (%).

2.2.2. "Coarse Aggregate Close Packing Theory"

In the theory of dense wrapping thickness of coarse aggregate, it is believed that large-pored concrete is formed by cement, sand, and other binding materials uniformly wrapping the coarse aggregate. The porosity of concrete is derived using the theoretical bulk density of the actual materials and the bulk density of fresh concrete [30].

The mix design formula is shown in Formula (2):

$$\frac{m_h}{m}\left(\frac{m_g}{\gamma_g} + \frac{m_{ggbs}}{\gamma_{ggbs}} + \frac{m_f}{\gamma_f} + \frac{m_r}{\gamma_r} + \frac{m_w}{\gamma_w} + \frac{m_s}{\gamma_s} + p\right) = 1 \quad (2)$$

In the above formula, m_g, m_s, m_{ggbs}, m_f, m_w, m_r represent the mass of coarse aggregate, fine aggregate, GGBS, FA, alkali solution, and RCP per 1 m^3 of concrete, respectively, with units of (kg); mh represents the theoretical bulk density of the mixture; ρ_{bulk} represents the actual bulk density of the concrete produced; units are (kg/m^3). γ_g, γ_s, γ_{ggbs}, γ_f, γ_w, and γ_r represent the apparent density of coarse aggregate, fine aggregate, GGBS, FA, alkali solution, and RCP, respectively; units are (kg/m^3), and p represents the connected porosity in sand-containing large-pore concrete; units are (%).

The cementitious material dosage gradient in this study was set at 300 kg/m^3, 350 kg/m^3, 400 kg/m^3, and 450 kg/m^3, with target porosities designed at 15%, 20%, and 25%. Thus, the study investigated the influence of different cementitious material dosages and porosities on the mechanical properties and permeability coefficient of CRHC. This study is based on the theoretical framework of the "closely packed filling theory" and the "tightly wrapped theory". Design the following mix proportions. By establishing an evaluation system that links target porosity (theoretical design value), theoretical porosity (numerical calculation value), and actual porosity (experimental measurement value), the deviation characteristics of porosity parameters under different theoretical models and their underlying causes were analyzed. This led to the selection of a mixed design theory with optimal porosity deviation control. The specific concrete mix designs are shown in Table 4.

Table 4. Concrete mix proportions.

Group	RAC (kg/m^3)	RFA (kg/m^3)	GGBS (kg/m^3)	FA (kg/m^3)	RCP (kg/m^3)	Aqueous Alkali (kg/m^3)	Target Porosity
ACRHC-1	1114	232.4	168	72	60	123.1	25%
ACRHC-2	1114	432.5	168	72	60	138.4	20%
ACRHC-3	1114	619.5	168	72	60	152.7	15%
ACRHC-4	1114	181.4	196	84	70	132.3	25%
ACRHC-5	1114	368.5	196	84	70	151.6	20%
ACRHC-6	1114	560.7	196	84	70	174.2	15%
ACRHC-7	1114	104.0	224	96	80	123.2	25%
ACRHC-8	1114	272.3	224	96	80	152.9	20%
ACRHC-9	1114	481.3	224	96	80	170.9	15%
ACRHC-10	1114	24.5	252	108	90	140.7	25%
ACRHC-11	1114	231.4	252	108	90	139.9	20%
ACRHC-12	1114	356.4	252	108	90	177.0	15%
PCRHC-1	1114	232.4	168	72	60	123.1	25%
PCRHC-2	1114	432.5	168	72	60	138.4	20%
PCRHC-3	1114	619.5	168	72	60	152.7	15%
PCRHC-4	1114	181.4	196	84	70	132.3	25%
PCRHC-5	1114	368.5	196	84	70	151.6	20%
PCRHC-6	1114	560.7	196	84	70	174.2	15%
PCRHC-7	1114	104.0	224	96	80	123.2	25%
PCRHC-8	1114	272.3	224	96	80	152.9	20%
PCRHC-9	1114	481.3	224	96	80	170.9	15%
PCRHC-10	1114	24.5	252	108	90	140.7	25%
PCRHC-11	1114	231.4	252	108	90	139.9	20%
PCRHC-12	1114	356.4	252	108	90	177.0	15%

Note: ACRHC refers to alkali-activated sand-containing hollow concrete prepared based on the "closely packed filling theory". PCRHC refers to alkali-activated sand-containing hollow concrete prepared based on the "tightly wrapped theory".

2.3. Sample Preparation and Methods

2.3.1. Pre-Treatment of RCP

In this study, a planetary cement test mill (Tianjin Yuan Guan Experimental Instrument Factory) was used to mechanically activate recycled concrete powder (RCP). The activation times were set at 0 min, 10 min, 20 min, and 30 min, with a single batch size of 2 kg. Based on this, in accordance with JG/T573-2020 [31] "Technical Specifications for the Application of Recycled Micropowder in Concrete and Mortar," RCP was used to prepare reference recycled concrete micropowder composite mortar (RCM) by replacing 30% of the reference cement by weight. The grinding times were denoted as RCM-0, RCM-10, RCM-20, and RCM-30. In subsequent experiments for preparing AARCPS-HC, the RCP with the highest activity index was used.

2.3.2. Preparation of AARCPS-HC

This experiment used the "cement-coated aggregate method" to prepare sand-containing large-pore concrete: first, the aggregate and half of the solution were added to the concrete mixing drum, and the mixture was stirred for 30 s to achieve surface wetting. After adding all cementitious materials, mixing continued for 40 s. The remaining solution was then introduced and blended for a final 30 s. The resulting mixture was poured into the mold in two layers of roughly equal thickness, with each layer compacted at its corners, sides, and surface using threaded steel bars, with approximately 15 taps evenly distributed. The second layer was then added, and the tamping operation was repeated. The preparation process of AARCPS-HC is shown in Figure 3.

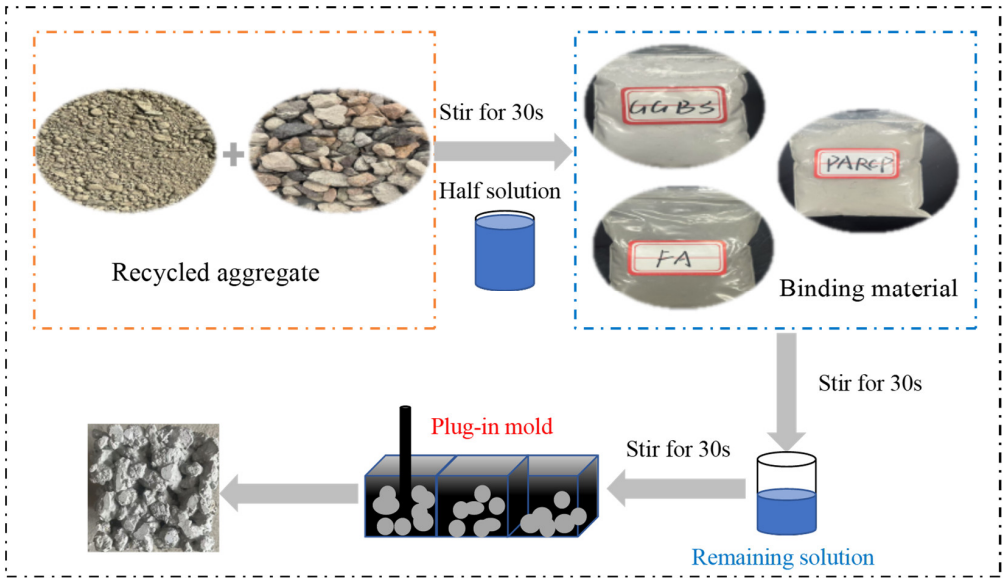

Figure 3. AARCPS-HC preparation process.

2.4. Test Methods

2.4.1. Activity Index Test

In accordance with JG/T573-2020 "Technical Specifications for the Application of Recycled Micropowder in Concrete and Mortar," this test employs an activity evaluation system based on the ratio of the 28-day compressive strength of the tested mortar to that of the reference mortar. It systematically characterizes the influence of mechanical activation duration on the RCP volcanic ash effect. The RCP group with the highest activity index is used to prepare AARCPS-HC.

2.4.2. Porosity Test

This test employs the "buoyancy method" to determine the porosity of large-pore concrete. According to Archimedes' principle, the volume of water displaced by the large-pore concrete specimen is its actual volume. The volume of effective open pores in the specimen is calculated by subtracting the displaced water volume from the specimen's apparent density. The formula is shown in Formula (3) [30]:

$$P = (1 - \frac{m_1 - m_2}{v}) 100 \quad (3)$$

m_1 denotes the mass of the specimen in air, in grams (g); m_2 denotes the mass of the specimen in water, in grams (g), and v denotes the apparent volume of the specimen (cm^3).

2.4.3. Compressive Strength Test

Compressive strength tests for alkali-activated sand-containing large-pore concrete at 3 d, 7 d, 14 d, and 28 d were conducted in accordance with GB/T 50081-2002 [32].

2.4.4. Freeze–Thaw Resistance Evaluation

Freeze–Thaw Resistance Evaluation was conducted in accordance with relevant provisions of GB/T 50082-2009 [33] "Test Methods for Long-Term Performance and Durability of Normal Concrete," employing the rapid freezing method for freeze–thaw cycles.

2.4.5. Permeability Coefficient Test

Permeability coefficient tests were conducted on alkali-activated sand-containing large-pore concrete in accordance with CJJ/T 135-2009 [34]. The test apparatus is shown in Figure 4.

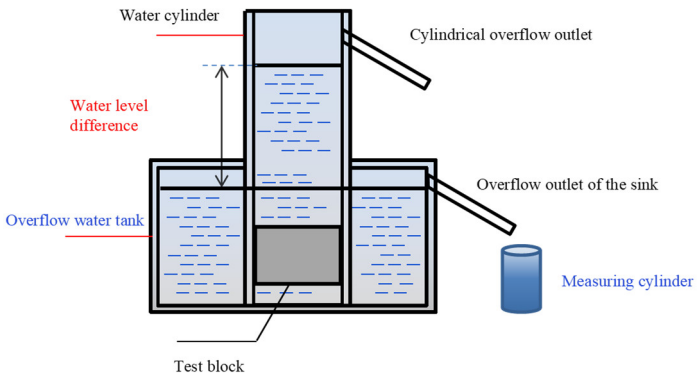

Figure 4. Permeability coefficient device.

The permeability coefficient in this test is determined according to the JC/T 2558-2020 [35] standard, as shown in Formula (4):

$$Kr = QL/AHt \quad (4)$$

This formula applies Darcy's Law to permeability testing of specimens, calculating the permeability coefficient of materials at a specific water temperature to indicate the ease or difficulty of water flow through the material. kr is defined as the permeability coefficient (in mm/s) of the specimen, measured at a water temperature of T °C, serving as the core metric for evaluating material permeability. Q denotes the volume of water discharged over time t (mm^3), requiring precise measurement through testing. L denotes the specimen thickness (mm), requiring measurement of the effective permeable thickness. A denotes the upper surface area of the specimen (mm^2), i.e., the effective permeable area in contact

with water. H denotes the water level difference (mm), serving as the source of hydraulic gradient driving water through the specimen. t denotes the permeation duration (s), which must align with the measurement time for water volume Q.

2.4.6. Microstructure and XRD Analysis

Samples were selected after crushing, and flake-shaped samples (with a diameter and thickness of less than 1 cm) were obtained. The microstructure of the AARCPS-HC interface transition zone was examined using scanning electron microscopy (SEM), while X-ray diffraction (XRD) was employed to determine the phase composition of the hydration products. These complementary techniques provided a comprehensive analysis of the concrete's characteristics. The hydration mechanism and interfacial strengthening mechanism of AARCPS-HC were revealed.

3. Results and Discussion

3.1. PARCP Activity Index Analysis

Figure 5 shows the 28-day strength of RCM and the activity index of PARCP under different grinding times. As shown in the figure, as the grinding time increases from 0 min to 30 min, the activity of RCP continues to grow, with the activity index increasing from 62.7% to 69.8%, representing an increase of 11.3%. Mechanical grinding causes the tetrahedral structure of SiO_2 within RCP to deform, transforming it into amorphous SiO_2. Additionally, a study by Du [36] noted that physical activation can also convert C-S-H in waste concrete into a more amorphous form through grinding, thereby enhancing volcanic ash activity. However, as the grinding time is extended, the specific surface area of RCP progressively increases, thereby enhancing its water absorption. A large amount of free water is absorbed, delaying the hydration reaction and resulting in reduced activity. Additionally, after mechanical grinding, the particle size of RCP decreases; the surface edges become rounded, and the particle shape becomes regular, enabling it to serve as ultra-fine aggregate in the cementitious system [37]. This helps improve particle grading.

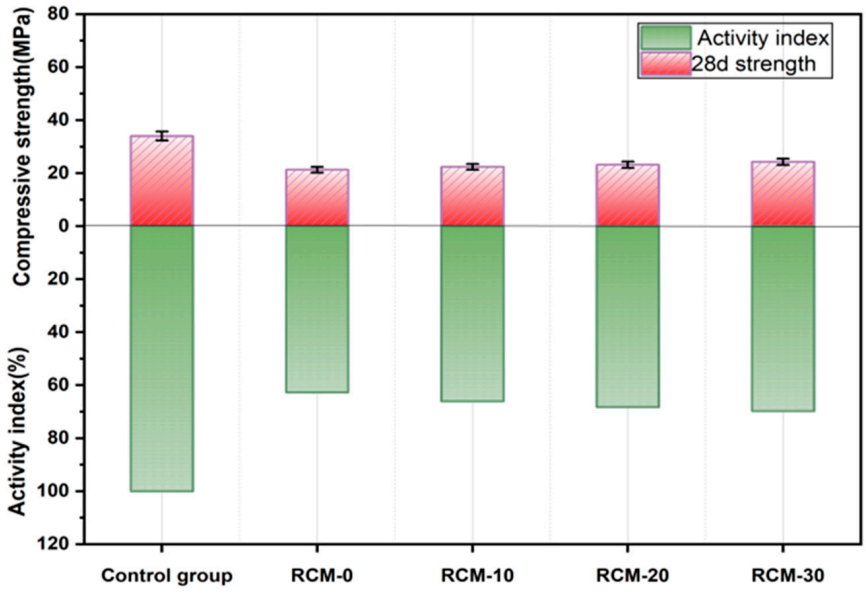

Figure 5. A 28-day strength of RCM and activity index of PARCP under different grinding times.

3.2. AARCPS-HC Pore Volume Deviation Analysis

3.2.1. ACRHC Pore Volume Analysis Based on the "Coarse Aggregate Tight Accumulation Theory"

Figure 6 shows the actual porosity, target porosity, and deviation between the calculated porosity and the porosity deviation ACRHC (which is based on the "coarse aggregate dense packing filling theory") under different amounts of cementitious materials. As shown in Figure 6, the measured porosity and the theoretical filling porosity exhibit similar trends with changes in sand content. When the target porosity is 15%, the maximum deviation between the measured porosity and the theoretical porosity reaches 3.6%, with an average deviation of 1.8%. When the target porosity is 20% and 25%, the average deviations are 3.2% and 1.5%, respectively. Although the theoretical porosity has a smaller deviation from the target porosity, there is still a certain error between the two. One reason is that in the actual preparation of large-pore concrete, the mortar wraps around the surface of the coarse aggregate, increasing the distance between the coarse aggregates [38,39], resulting in volume expansion. This causes the measured porosity of the concrete to be greater than the theoretical porosity. Additionally, the aggregates were not sufficiently compacted during the molding process, indicating that the apparent volume of macro-porous concrete prepared using a mix ratio of 1 m^3 is actually greater than 1 m^3, as shown in Figure 6.

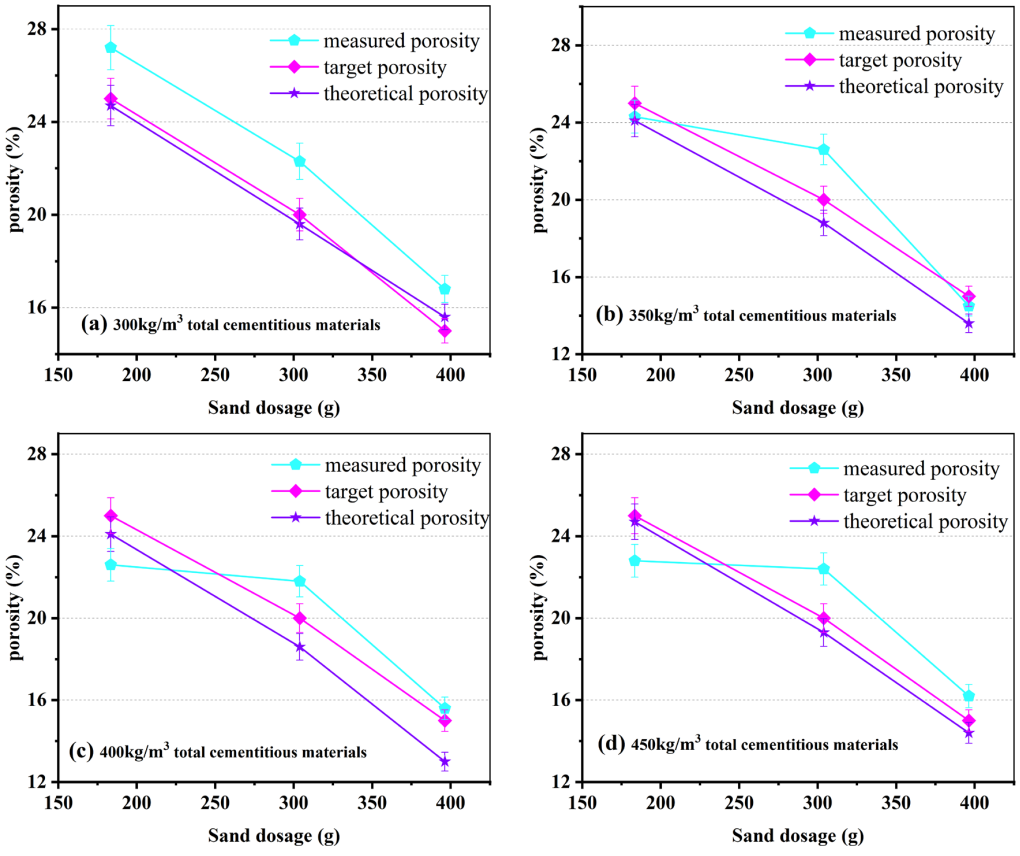

Figure 6. Porosity deviation under different amounts of cementitious materials—"Coarse aggregate close packing theory": (**a**) 300 kg/m^3 total cementitious materials, (**b**) 350 kg/m^3 total cementitious materials, (**c**) 400 kg/m^3 total cementitious materials, (**d**) 450 kg/m^3 total cementitious materials.

On the other hand, the specimens used in this experiment were 100 mm × 100 mm × 100 mm cubic specimens, and the mold walls produce a "sidewall effect." The "sidewall effect" refers to the phenomenon in concrete structures, where, when the concrete boundaries are subjected to external loads, strong reaction forces and bending strains occur at the

sidewalls. This phenomenon affects the strength, load-bearing capacity, and stability of concrete structures. The presence of the "edge wall effect" alters the accumulation pattern of coarse aggregates enclosed by the mortar at the boundaries and within the specimen. At the boundaries, the aggregates are subjected to pressure from only one direction, resulting in incomplete filling of some pores at the boundaries and an increase in porosity [30].

To verify the deviation between the measured porosity and the target porosity caused by the "edge wall effect," the specimens were sliced and photographed, and the images were binarized using Matlab software. Specimens with target porosities of 15%, 20%, and 25% at 400 kg/m^3 were selected for slicing (background detection threshold set to 250; pore segmentation threshold set to 0.3). The influence range was considered to be the maximum particle size of coarse aggregate [40,41]. The maximum particle size of coarse aggregate used in this experiment was 16 mm, and the influence range was taken as 20 mm during analysis and processing. The sectioned images and binarized images are shown in Figure 7.

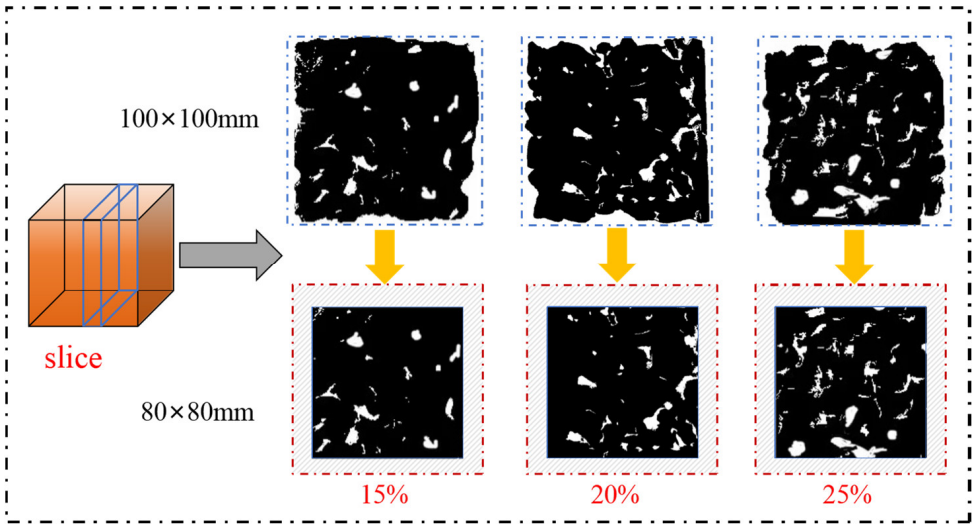

Figure 7. Cross-section of ACRHC and binarization processing diagram.

As shown in Figure 7, after image processing, the theoretical porosity of the cross-section with dimensions of 100 mm × 100 mm is larger than that of the cross-section with dimensions of 80 mm × 80 mm. This indicates that the presence of the "edge effect" causes deviations in the porosity of the specimens. The method based on the "coarse aggregate close-packing theory" for calculating the target porosity of alkali-activated sand-containing coarse-porous concrete is unreliable.

3.2.2. Porosity Analysis Based on the "Coarse Aggregate Close Packing Theory"

Figure 8 shows the deviations between the actual porosity of PCRHC and the target porosity and theoretical porosity. As can be seen in the figure, the measured porosity of PCRHC and the theoretical porosity exhibit a basic trend similar to that of ACRHC. When the target porosity is 15%, the maximum deviation between the measured porosity and the theoretical porosity is 2.1%, with an average deviation of 1.4%. When the target porosity is 20% and 25%, the maximum deviations are 1.3% and 1.2%, respectively, with average deviations of 1.2% and 0.8%. As the sand content increases, the porosity gradually decreases. The deviation between the measured porosity and the theoretical porosity of PCHRC is relatively small, with the minimum deviation reaching 0.2%, the maximum deviation being 2.1%, and the average deviation being 1.1%. Compared with the porosity deviation of ACRHC, the maximum deviation has decreased by 42.1%. This indicates

that the calculation method based on this theory can make the measured porosity of alkali-activated sand-containing large-pore concrete approach the theoretical porosity.

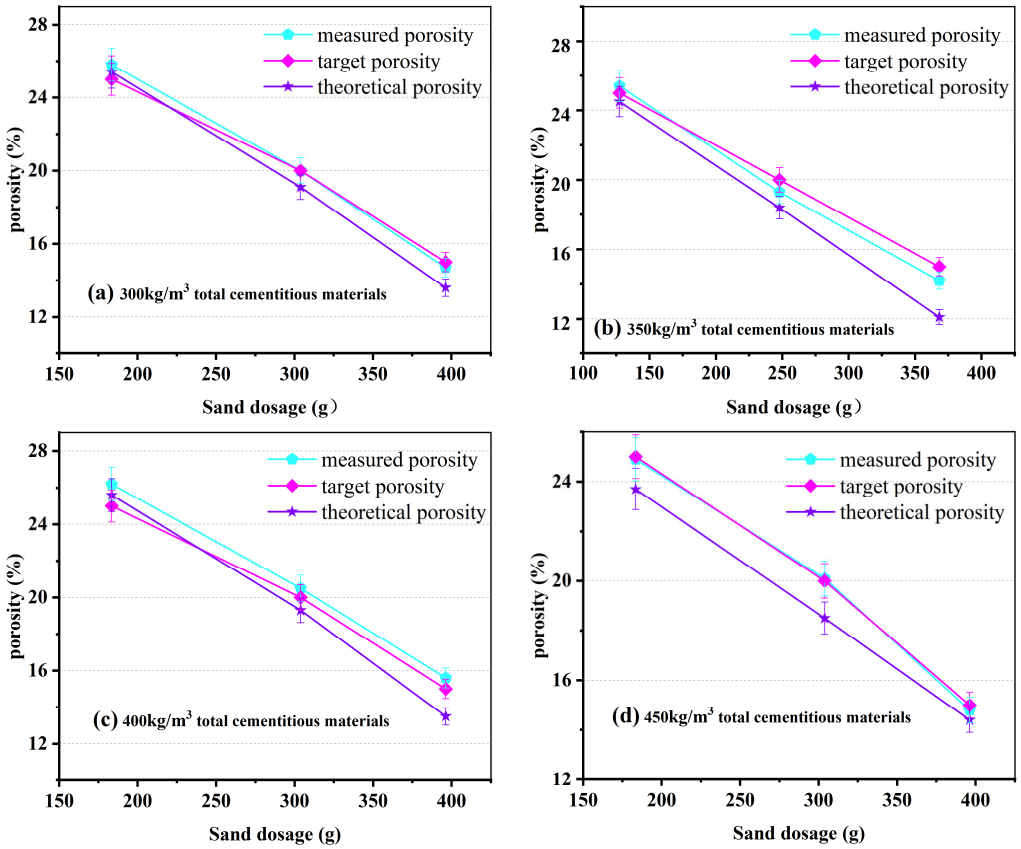

Figure 8. Porosity deviation under different cementitious material content—'Coarse aggregate tightly wrapped theory': (**a**) 300 kg/m^3 total cementitious materials, (**b**) 350 kg/m^3 total cementitious materials, (**c**) 400 kg/m^3 total cementitious materials, (**d**) 450 kg/m^3 total cementitious materials.

This theory takes into account the increased surface thickness caused by the mortar enveloping the aggregates, prepares large-pore concrete using a 1 m^3 mix ratio, and considers the volume expansion of the concrete and the insufficient compaction of the internal aggregates. This results in the actual density of the concrete not reaching its theoretical density, which is another factor contributing to the porosity deviation. As shown in Figure 9, indicates aggregate accumulation and tightly packed theoretical pore space.

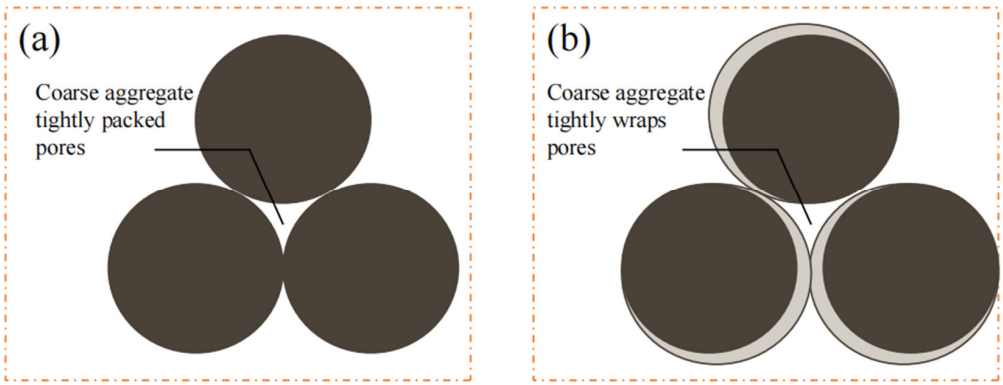

Figure 9. Aggregate accumulation and tightly packed theoretical pore space: (**a**) Coarse aggregatetightly packed pores; (**b**) Coarse aggregatetightly wraps pores.

3.2.3. Effect of Total Slurry Volume on Porosity

Under the condition of ensuring good working performance, a linear relationship between the slurry and porosity was obtained, as shown in Figure 10. The linear relationship formula is as follows:

$$Y = -0.026X + 41.78$$

$$R^2 = 0.94$$

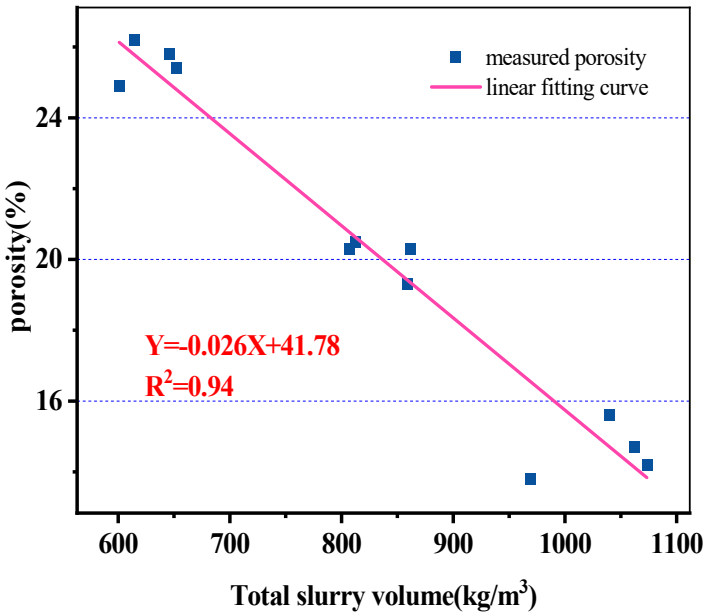

Figure 10. Linear relationship between total slurry volume and porosity.

As shown in Figure 10, while ensuring good workability, the measured porosity of PCRHC decreases as the total mortar volume increases, and the two are highly positively correlated. This is because, as the amount of mortar used increases, the amount of mortar used to fill the pores tightly wrapped around the coarse aggregate also increases, leading to a decrease in the measured porosity. For ACRHC, each increase of 50 kg/m^3 in mortar reduces porosity by approximately 1.3%.

The pores in PCRHC primarily originate from skeletal pores formed by the accumulation of coarse aggregate and internal micro-pores after mortar hardening. When the mortar volume increases, more mortar fills the gaps between coarse aggregates, reducing macro-porosity, and the slurry envelops the aggregates more fully, reducing defects in the interface transition zone and lowering the microporosity [19,42]. In ordinary concrete, excessive slurry may cause aggregate suspension, increasing the risk of shrinkage and cracking; however, due to the low shrinkage characteristics of alkali-activated cementitious materials in ACRHC, an increase in slurry has a minimal impact on volume stability [43,44].

3.3. Mechanical Performance Analysis of PCRHC

3.3.1. Effect of Porosity on Mechanical Performance

Figure 11 presents the compressive strength of PCHRC as a function of pore volume fraction, with results compared across different cementitious material dosages. As the porosity increases, the compressive strength of PCHRC gradually decreases. Taking a cementitious material dosage of 400 kg/m^3 as an example, when the porosity increases from 15% to 20% and 25%, the 28-day compressive strength increases from 17.6 MPa to 15.7 MPa and 13.4 MPa, representing increases of approximately 10.8% and 23.4%, respectively. This is because the large-pore concrete primarily transmits external forces through contact

points between aggregates and small-area contact surfaces. When subjected to loads, stress concentration occurs at the contact points between internal aggregate particles [45,46], making them prone to fracture. An increase in porosity reduces the number of bonding surfaces and contact points, thereby damaging the strength of the large-pore concrete.

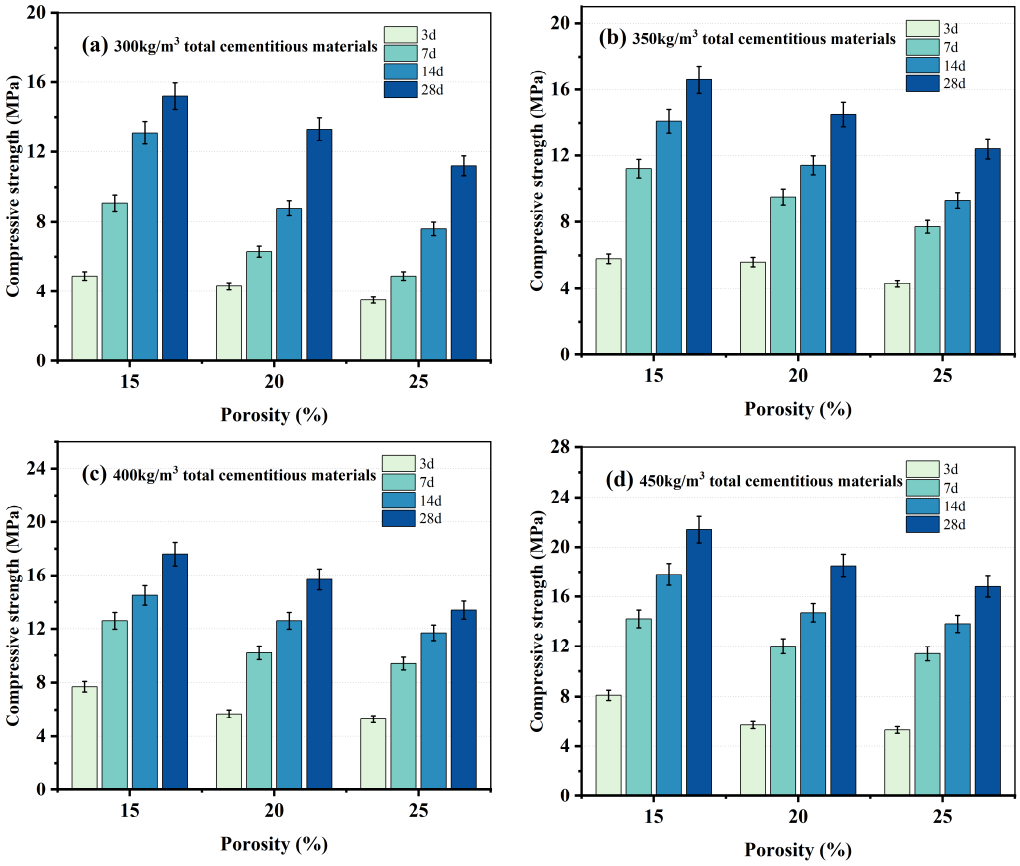

Figure 11. Compressive strength of PCHRC with different porosities under different cementitious material contents: (**a**) 300 kg/m^3, (**b**) 350 kg/m^3, (**c**) 400 kg/m^3, (**d**) 450 kg/m^3.

3.3.2. Influence of Binder Material Quantity on Mechanical Properties

Figure 12 shows the relationship between compressive strength and different cementitious material content in PCHRC under the same porosity. It indicates that as the cementitious material content increases, the compressive strength of PCHRC gradually improves. This is because the increased cementitious material promotes the hydration reaction, leading to an increase in hydration products and gels, which makes the internal structure of the concrete denser, thereby facilitating the development of compressive strength. At porosities of 15%, 20%, and 25%, within the range from 300 kg/m^2 to 450 kg/m^2 of cementitious materials, the 28-day compressive strength of PCHRC increased by 50%, 39%, and 41%, respectively. Additionally, compared to the preparation of large-pore concrete using NCA, the increase in cementitious material content has a more significant effect on enhancing the strength of RCA large-pore concrete. A research report by Wang [47] stated that the surface of recycled concrete aggregate (RCA) is rich in active substances such as $Ca(OH)_2$ due to the attachment of a large amount of old mortar. After reacting with the alkaline components in the alkali-activated cementitious material, it can in situ generate a calcium carbonate ($CaCO_3$) coating. This mineralized product effectively fills the pore structure on the aggregate surface, thereby enhancing the overall performance of RCA through physical densification [48]. However, due to the poor quality of the aggregate, its overall strength remains lower than that of natural aggregate concrete. Soon [49] et al. used

RCA to replace NCA (20%, 40%, 60%, 80%) to prepare hollow concrete, and found that the replacement of RCA reduced the compressive, flexural, and splitting strengths of the hollow concrete. This is due to the high water absorption of RCA, which reduces the water required for hydration reactions, decreases the formation of hydration products, and leads to poor bonding between the aggregate and the paste, resulting in reduced strength.

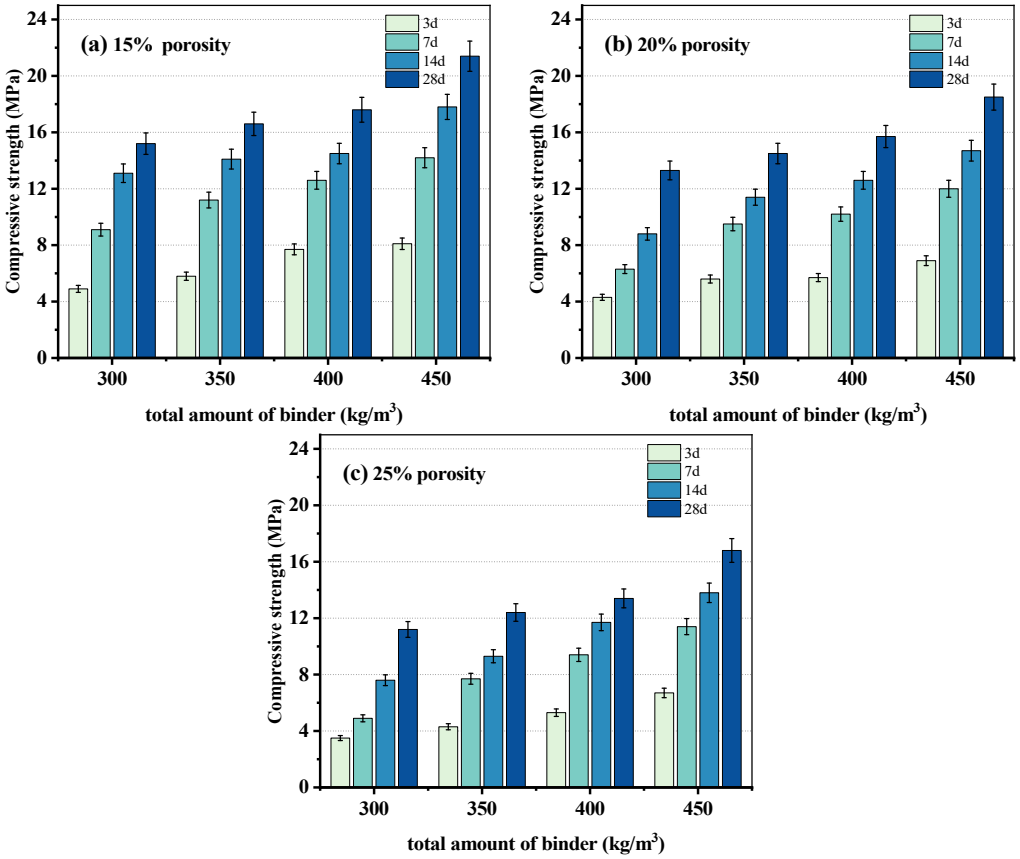

Figure 12. Compressive strength of PCHRC with different amounts of cementitious materials at the same porosity: (**a**) 15%, (**b**) 20%, (**c**) 25%.

3.4. Permeability Coefficient Analysis of PCRHC

Figure 13 shows the permeability coefficient of ACRHC at different porosities. At a porosity of 15%, the permeability coefficient of ACRHC ranges from 5.2 to 5.7 mm/s. Although there are many pores at this porosity, some pores may be partially filled with mortar, resulting in restricted flow paths. When the porosity reaches 25%, the permeability coefficient increases to 6.9–7.6 mm/s, representing a 33% increase. As porosity increases, the proportion of effectively connected pores increases, significantly reducing hydraulic resistance [50–52]. According to the data, the permeability coefficient and porosity have a linear positive correlation, but the correlation coefficient is small. This is because the mineral admixture used in this study can not only effectively fill the pores between coarse aggregates, but also promote the dispersion of particles and disrupt their flocculation structure. This dual effect of filling and dispersion jointly optimizes the microstructure of the material, thereby affecting its macroscopic properties. Yu observed the pore characteristics of the permeable concrete through CT scanning. The study indicated that as the particle size of the aggregate increased; the content of small pores within 20 mm^2 gradually decreased, while the content of large pores above 50 mm^2 increased. As a result, the permeability of the permeable concrete increased [53]. Shan's research found that the amount of water in

the pores within the permeable concrete and the maximum pore diameter would increase as the porosity increased [52].

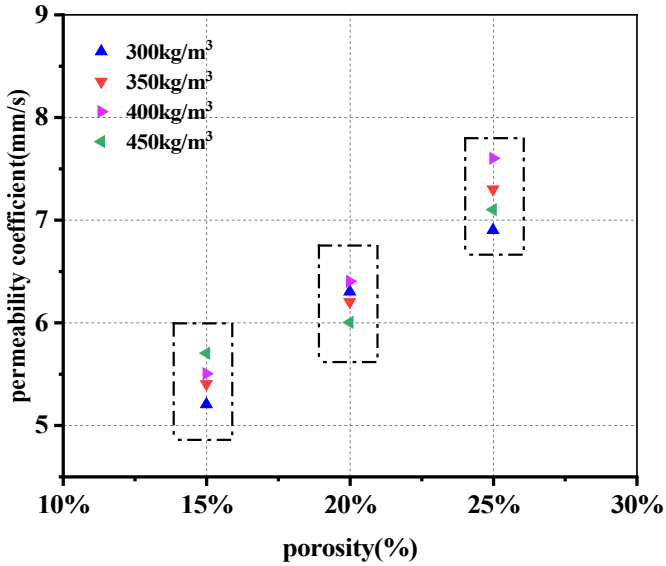

Figure 13. Permeability coefficient of ACRHC under different porosities.

3.5. AASCRHC Freeze Resistance Performance Evaluation

Effect of Binder Content and Porosity on Freeze–Thaw Resistance

As shown in Figure 14, the total cementitious material content is 400 kg/m^3. After 25 freeze–thaw cycles, the mass loss rates at target porosities of 25%, 20%, and 15% were 1.98%, 2.54%, and 2.89%, respectively. When the cementitious material content was 450 kg/m^3, the mass loss rates reached 1.23%, 2.01%, and 2.64%, representing decreases of 36.5%, 20.9%, and 13.8%, respectively. At the same porosity, increasing the cementitious material content enhances the strength of the hardened cement paste layer enveloping the coarse aggregate surfaces, thereby improving the material's inherent resistance to freeze–thaw damage. Furthermore, as porosity increases, both the mass loss rate and compressive strength loss rate of macro-porous concrete rise, deteriorating its freeze–thaw resistance. This primarily occurs because higher porosity allows more freezeable water to penetrate the macro-porous ecological concrete. During temperature-induced freezing, the resulting volumetric expansion generates greater pressure, causing more severe damage to sand-containing macro-porous concrete.

3.6. PCRHC Microstructural Analysis

3.6.1. SEM Analysis

Figure 15 shows the SEM image of AARCPS-HC at 28 days of age. In the samples prepared using physically activated recycled micro-powder, micro-cracks and a fibrous network morphology of C-(A)-S-H gel can be clearly observed. This is attributed to the CaO, SiO_2, and Al_2O_3 components in GGBS and FA undergoing bond breakage and of Si–O–Si and Si–O–Al bonds under the influence of an alkaline medium; simultaneously, the introduction of physically activated recycled micro-powder (PARCP) significantly increases the active SiO_2 content in the system, promoting the participation of more OH^- in the gelation reaction and generating hydration products such as C-S-H and C-A-S-H [54,55]. It is worth noting that while the inclusion of PARCPs improves material composition by increasing the number of products in the interface transition zone, it also leads to the formation of microcrack defects. Microscopic observations indicate that no obvious unreacted materials are present on the RCP surface, which is closely related to the microscopic

mechanism of being densely encapsulated by hydrated gel [54,56]. This is because RCP is encapsulated internally by the already formed gel material, thereby forming a dense microscopic structure. Meanwhile, some unreacted RCP particles serve as new nucleation sites, promoting the formation of new products on the RCP particle surface.

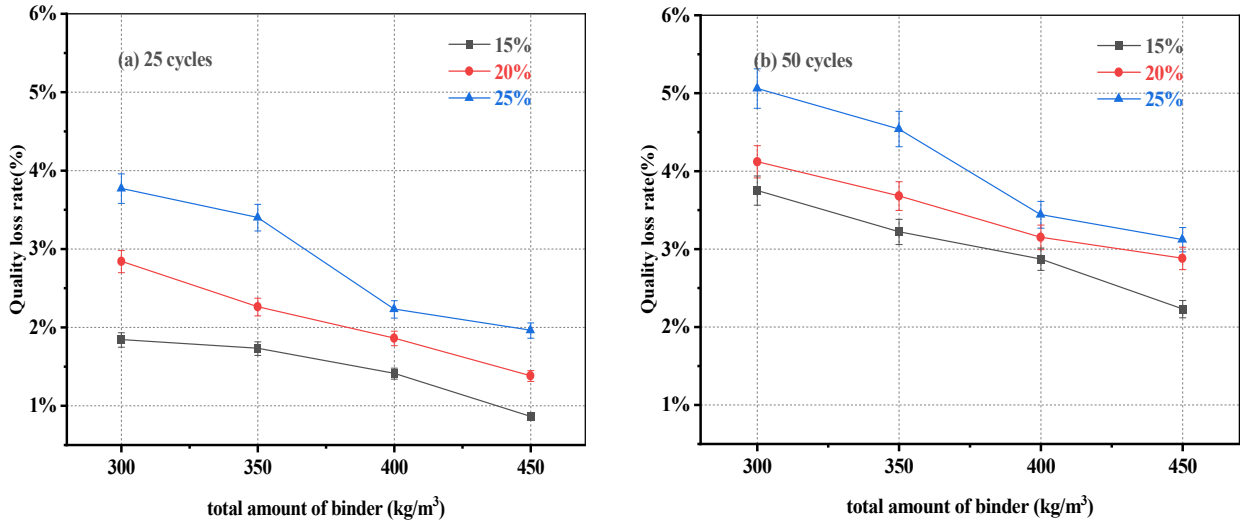

Figure 14. Freeze–thaw quality loss rate of PCHRC under different cementitious material dosages and porosities: (**a**) 25 cycles, (**b**) 50 cycles.

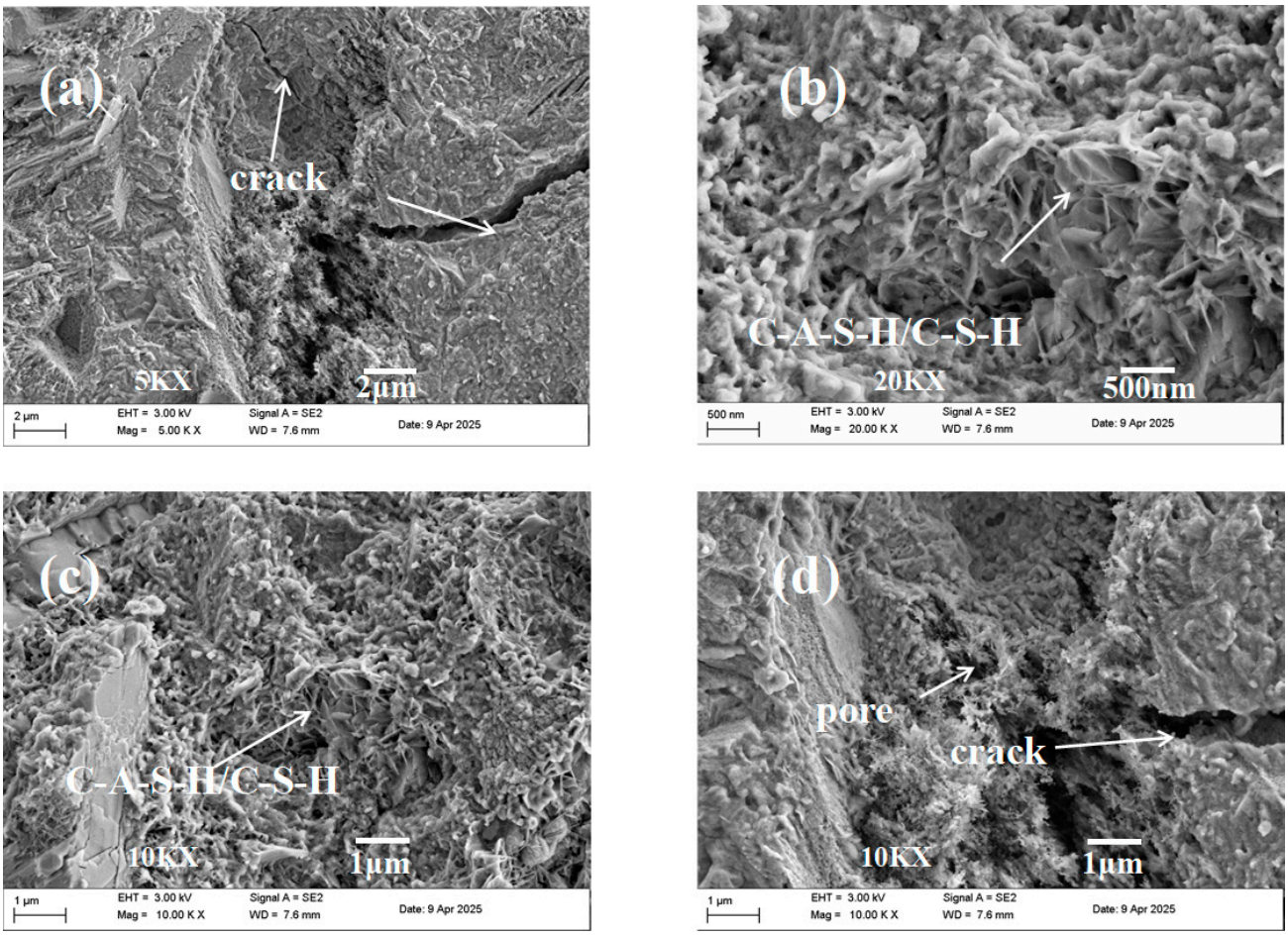

Figure 15. SEM image of AARCPS-HC at 28 days of age.

3.6.2. XRD Analysis

Figure 16 shows the XRD spectrum of the hydration products of alkaline-activated sand-containing hollow concrete produced after the addition of PARCP. The detection of a semi-crystalline phase generated by the base-activated reaction and the presence of unreacted phases in the raw materials was shown by Su et al. [57]. The XRD spectrum indicates that quartz and muscovite are the primary crystalline phases, primarily derived from the recycled sand used to adjust the porosity. Gel-like substances such as calcium silicoaluminate hydrate (C-A-S-H) and calcium silicate hydrate (C-S-H) were also detected. The sources of $CaCO_3$ include old cement mortar adhering to the surface of recycled aggregates and the reaction between $Ca(OH)_2$ and CO_2 during the physical activation of RCP.

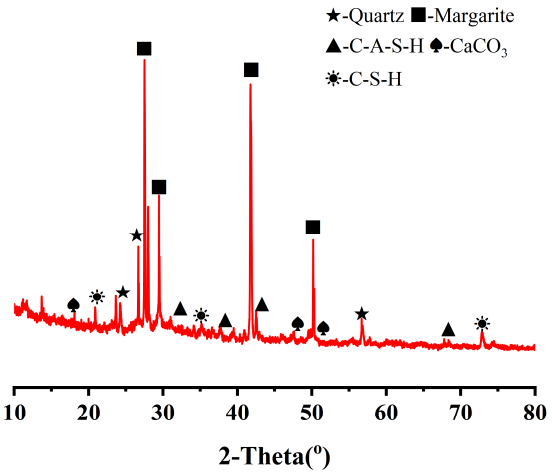

Figure 16. XRD pattern of the hydration product of AASCRHC at 28 days of age.

3.7. Discussion

This study innovatively employs physically activated recycled concrete powder (RCP) as an auxiliary cementitious material, incorporating both the "coarse aggregate close-packed filling theory" (volume method) and the "coarse aggregate close-wrapped filling theory" (bulk density method) to establish a preparation system for alkali-activated sand-containing porous concrete. By establishing a three-dimensional evaluation model of "measured porosity–theoretical porosity–target porosity," the study systematically revealed the formation mechanism of porosity deviations under different aggregate packing patterns. Combining Matlab image binarization technology with spatial topological analysis of concrete sections, the study quantitatively validated the heterogeneous porosity distribution characteristics in the interface transition zone caused by the "edge wall effect."

4. Conclusions

This study innovatively employs recycled construction waste micro-powder (RCP) as the core raw material to systematically establish the preparation system for alkali-activated sandy macro-porous concrete (AASCRHC). By verifying the evolution patterns of actual/theoretical porosity of A AASCRHC under different theoretical frameworks—including the theory of coarse aggregate close-packing and the theory of pore formation—the study deeply elucidates its strength-gradient response mechanism and micro-hydration evolution characteristics. The research findings not only provide an innovative solution for the high-value utilization of construction waste but also establish a quantitative correlation model linking "pore structure–mechanical properties–interface effects," thereby providing theoretical support and practical guidance for the large-scale application of AARCPS-HC in

green building engineering. Based on the aforementioned research findings, the following core conclusions are drawn:

1. AASCRHC, prepared based on the coarse aggregate tight wrapping and filling theory (bulk density method), demonstrates excellent pore control performance, with an average deviation between actual and theoretical porosity of only 1.1%, representing a 42.1% reduction in maximum porosity deviation compared to traditional concrete (ACRHC). Research has found that the edge effect, which alters the differential accumulation patterns of the paste-aggregate interface at the specimen boundaries and interior, is a key factor influencing pore volume deviation.

2. Within the range of 300 kg/m^2 to 450 kg/m^2 of cementitious materials, the 28-day compressive strength of AASCRHC increased by 50%, 39%, and 41%. When the cementitious material content was 400 kg/m^3, the porosity increased from 15% to 20% and 25%, resulting in approximately 17.2% and 31.3% increases in 28-day compressive strength.

3. The permeability coefficient increases non-linearly with porosity. When porosity increased from 15% to 25%, the permeability coefficient improved by 33% (from 5.2–5.7 mm/s to 6.9–7.6 mm/s), primarily due to an increase in interconnected pores. However, the actual increase was lower than the theoretical value, indicating that pore connectivity remains a key limiting factor.

4. Increasing the cementitious material content (e.g., from 400 kg/m^3 to 450 kg/m^3) enhances freeze–thaw resistance by strengthening the cement paste (reducing mass loss by up to 36.5%). However, increasing porosity exacerbates freeze–thaw damage by accumulating more free water. Therefore, in practical engineering applications, cementitious material content should be maximized while maintaining ecological porosity to optimize concrete durability.

5. During the alkali activation process, Si–O–Si and Si–O–Al bonds undergo depolymerization and repolymerization, forming a three-dimensional network C-(A)-S-H gel structure. This corresponds to the fibrous gel morphology observed by SEM. Meanwhile, microcracks between gels originate from volume shrinkage during the reaction and stress differences at the aggregate–gel interface. Microscopic analysis indicates that unreacted RCP particles act as nucleation sites in the hydration system, promoting the directed growth of new hydration products on their surfaces. The incorporation of PARCP improves material composition by increasing the number of products in the interfacial transition zone, but it also leads to the formation of microcracks, resulting in a typical "enhancement-damage" dual-effect mechanism.

Author Contributions: Conceptualization, Y.G. and Q.L.; methodology, Y.G., Z.Z. and M.C.; validation, Z.Z.; formal analysis, W.L. and Z.Z.; investigation, G.Y.; resources, X.X. and C.S.; data curation, W.L. and Z.Z.; writing—original draft preparation, Y.G. and Z.Z.; writing—review and editing, Y.G. and W.L.; visualization, W.L.; supervision, Q.L. and M.C.; project administration, G.Y., X.X. and C.S.; funding acquisition, Q.L. All authors have read and agreed to the published version of the manuscript.

Funding: This research was funded by National Natural Science Foundation of China [grant number 52478262]; Qingdao Natural Science Foundation Youth Project [grant number 23-2-1-105-zyyd-jch]; Shandong Province City-level School Enterprise Cooperation Project [grant numbers 2425282, 2425244, 2424360, 2423272]. The APC was funded by National Natural Science Foundation of China [grant number 52478262].

Data Availability Statement: All data, models, or code that support the findings of this study are available from the corresponding author upon reasonable request.

Conflicts of Interest: Author Changhai Shao was employed by Shandong Guanrunjia Environmental Protection New Materials Co., Ltd. The remaining authors declare that the research was conducted in the absence of any commercial or financial relationships that could be construed as a potential conflict of interest.

References

1. Wu, H.; Weng, X.; Chen, R.; Du, L.; Li, Y.; Liu, W.; Liu, S.; Yu, B.; Bao, Z. Generation characteristics and disposal paths of construction waste in public building project, A case study. *Clean. Waste Syst.* **2025**, *10*, 100211. [CrossRef]
2. Gao, Q.; Li, X.G.; Jiang, S.Q.; Lyu, X.J.; Gao, X.; Zhu, X.N.; Zhang, Y.Q. Review on zero waste strategy for urban construction and demolition waste, Full component resource utilization approach for sustainable and low-carbon. *Constr. Build. Mater.* **2023**, *395*, 132354. [CrossRef]
3. Hou, H.; Su, L.; Guo, D.; Xu, H. Resource utilization of solid waste for the collaborative reduction of pollution and carbon emissions, Case study of fly ash. *J. Clean. Prod.* **2023**, *383*, 135449. [CrossRef]
4. Sagan, J.; Mach, A. Construction waste management, Impact on society and strategies for reduction. *J. Clean. Prod.* **2025**, *486*, 144363. [CrossRef]
5. Ma, X.; Hu, H.; Luo, Y.; Yao, W.; Wei, Y. A carbon footprint assessment for usage of recycled aggregate and supplementary cementitious materials for sustainable concrete, A life-cycle perspective in China. *J. Clean. Prod.* **2025**, *490*, 144772. [CrossRef]
6. Zhao, G.; Guan, H.; Yan, H.; Ruan, Y.; Han, Y.; Pan, X.; Tian, J.; Liu, B. An innovative sustainable solution, Recycling shield-discharge waste soil as fine aggregate to produce eco-friendly geopolymer-based flowable backfill materials. *Environ. Technol. Innov.* **2024**, *36*, 103857. [CrossRef]
7. Wu, L.; Majid, A.; Tang, Q.; Sun, Z.; Cao, Y. Effect of calcium phosphate modification on the interfacial transition zone of recycled aggregate and concrete. *Cem. Concr. Compos.* **2025**, *157*, 105872. [CrossRef]
8. Liu, Q.; Cheng, X.; Sun, C.; Jin, C.; Tam, V.W. Impact of carbonization and aggregate properties on modeled recycled concrete, Mechanical characteristics, stress concentration and damage evolution. *Constr. Build. Mater.* **2025**, *467*, 140327. [CrossRef]
9. Abbas, N.S.; Qureshi, I.M. Influence on the durability properties of concrete after incorporating different types of recycled aggregates, A review. *Prog. Eng. Sci.* **2024**, *1*, 100026. [CrossRef]
10. Brasileiro, K.P.T.V.; de Oliveira Nahime, B.; Lima, E.C.; Alves, M.M.; Ferreira, W.P.; dos Santos, I.S.; Filho, C.P.B.; dos Reis, I.C. Influence of recycled aggregates and silica fume on the performance of pervious concrete. *J. Build. Eng.* **2024**, *82*, 108347. [CrossRef]
11. Ma, Y.; You, Q.; Li, J.; Lu, C.; Yin, J.; Li, H.; Meng, W.; Liu, Z.; Wang, Y.; Gao, X.; et al. Study on the use of CO2 to strengthen recycled aggregates and pervious concrete. *Constr. Build. Mater.* **2024**, *418*, 135372. [CrossRef]
12. Chen, Z.; Zhang, J.; Cao, C.S.; Song, Y.; Chen, Z. Surface reinforcement of recycled aggregates (RAs) by geopolymer and quantifying its morphological characteristics by machine learning. *J. Build. Eng.* **2024**, *91*, 109731. [CrossRef]
13. Ren, X.; Yang, J.; Chen, W.; Huang, Y.; Wang, G.; Niu, J.; Wu, J. Effect of recycled concrete powder-cement composite coating modification on the properties of recycled concrete aggregate and its concrete. *Constr. Build. Mater.* **2024**, *444*, 137860. [CrossRef]
14. Paramveer, S.; Kanish, K. Developing geopolymer concrete using fine recycled concrete powder and recycled aggregates. *Mag. Concr. Res.* **2024**, *76*, 1091–1105. [CrossRef]
15. Fatiha, A.; Karim, E.; Mhamed, A.; Abed, F. Enhancing performance of recycled aggregate concrete with supplementary cementitious materials. *Clean. Mater.* **2025**, *15*, 100298. [CrossRef]
16. Yao, T.; Tian, Q.; Zhang, M.; Qi, S.; Wang, C.; Ruan, M. Laboratory investigation of foamed concrete prepared by recycled waste concrete powder and ground granulated blast furnace slag. *J. Clean. Prod.* **2023**, *426*, 139095. [CrossRef]
17. Wang, D.; Lu, C.; Zhu, Z.; Zhang, Z.; Liu, S.; Ji, Y.; Xing, Z. Mechanical performance of recycled aggregate concrete in green civil engineering, Review. *Case Stud. Constr. Mater.* **2023**, *19*, e02384. [CrossRef]
18. Soni, N.; Shukla, K.D. Analytical study on mechanical properties of concrete containing crushed recycled coarse aggregate as an alternative of natural sand. *Constr. Build. Mater.* **2021**, *266*, 120595. [CrossRef]
19. Wang, Y.; Zhu, Z.; Cao, R.; Xu, L.; Huang, B. Insights into the properties of pervious concrete modified with polymers and fine aggregate. *Case Stud. Constr. Mater.* **2025**, *22*, e04627. [CrossRef]
20. Li, J.; Zha, W.; Lv, W.; Xu, T.; Wang, B.; Wang, B. Mechanical properties and sulfate resistance of basalt fiber-reinforced alkali-activated fly ash-slag-based coal gangue pervious concrete. *Case Stud. Constr. Mater.* **2024**, *21*, e03961. [CrossRef]
21. Singh, A.; Bhadauria, S.S.; Thakare, A.A.; Kumar, A.; Mudgal, M.; Chaudhary, S. Durability assessment of mechanochemically activated geopolymer concrete with a low molarity alkali solution. *Case Stud. Constr. Mater.* **2024**, *20*, e02715. [CrossRef]
22. Sun, Z.; Lin, X.; Vollpracht, A. Pervious concrete made of alkali activated slag and geopolymers. *Constr. Build. Mater.* **2018**, *189*, 797–803. [CrossRef]
23. Li, B.; Qin, Z.; Song, N.; Li, Y.; Zhang, J.; Wang, S. Coupling effect of silica fume and steel fiber on the mechanical properties and microstructures of alkali-activated slag recycled aggregate concrete. *J. Build. Eng.* **2025**, *103*, 112099. [CrossRef]

24. Tan, Y.; He, Y.; Cui, X.; Liu, L. Design and performance optimization of alkali-activated waste coal bottom ash/slag porous concrete. *Constr. Build. Mater.* **2022**, *359*, 129413. [CrossRef]
25. Zheng, X.; Pan, J.; Easa, S.; Fu, T.; Liu, H.; Liu, W.; Qiu, R. Utilization of copper slag waste in alkali-activated metakaolin pervious concrete. *J. Build. Eng.* **2023**, *76*, 107246. [CrossRef]
26. Kong, X.; Yao, Y.; Kai, M.; Guan, Y.; Ding, X.; Gu, Z.; Liu, J. The assessment of the mechanical and durability properties of mortar prepared with carbon dioxide-treated recycled concrete-brick powder. *Constr. Build. Mater.* **2025**, *466*, 140305. [CrossRef]
27. Deng, Y.; Wu, L. Effect of recycled concrete fine powder after calcination on the properties of autoclaved aerated concrete. *Case Stud. Constr. Mater.* **2024**, *20*, e02961. [CrossRef]
28. Zhang, D.; Zhang, S.; Huang, B.; Yang, Q.; Li, J. Comparison of mechanical, chemical, and thermal activation methods on the utilisation of recycled concrete powder from construction and demolition waste. *J. Build. Eng.* **2022**, *61*, 105295. [CrossRef]
29. Ma, Z.; Jiang, Y.; He, J.; Shen, P.; Qin, Q.; Gu, Z.; Li, J.; Poon, C.S. Revealing the connection between carbonation regimes and early pozzolanic reactivity of recycled concrete powder, Impact of composition and microstructure. *Cem. Concr. Res.* **2024**, *186*, 107697. [CrossRef]
30. Xu, C.; Li, Q.; Wang, P.; Fan, Q.; Kong, Z.; Wang, L.; Yue, G.; Zheng, S.; Shao, C.; Guo, Y. Theoretical porosity design, mechanical properties, and durability of large-pore sandy recycled concrete. *Case Stud. Constr. Mater.* **2024**, *21*, e03655. [CrossRef]
31. *JG/T 573-2020*; Recycled Fine Powder Used in Concrete and Mortar. China Quality Standard Press: Beijing, China, 2020.
32. *GB/T 50081-2002*; Standard for Test Method of Mechanical Properties on Ordinary Concrete. National Standard of the People's Republic of China: Beijing, China, 2003.
33. *GB/T 50082-2009*; Standard for Test Methods of Long-Term Performance and Durability of Ordinary Concrete. Ministry of Housing and Urban-Rural Development of the People's Republic of China: Beijing, China, 2009.
34. *CJJ/T 135-2009*; Technical Specification for Permeable Brick Pavement. Ministry of Housing and Urban-Rural Develop-ment of the People's Republic of China: Beijing, China, 2009.
35. *JC/T 2558-2020*; Pervious Concrete. Ministry of Industry and Information Technology of the People's Republic of China: Beijing, China, 2020.
36. Du, J.; Zhang, T.; Chen, P.; Guo, Y.; Zhan, B.; Wei, J.; Yu, Q. Phase separation of recycled concrete powder during grinding and consequent influences on its hydration behaviors in cement paste. *Cem. Concr. Compos.* **2023**, *142*, 105203. [CrossRef]
37. Ma, Z.; Hu, R.; Yao, P.; Wang, C. Utilizing heat-mechanical synergistic treatment for separating concrete waste into high-quality recycled aggregate, active recycled powder and new concrete. *J. Build. Eng.* **2023**, *68*, 106161. [CrossRef]
38. Xiong, B.; Li, Y.; Chen, B.; Lu, X.; Gao, H.; Jia, S. Influence of distribution of paste coating thickness on performance of pervious concrete. *Constr. Build. Mater.* **2025**, *458*, 139602. [CrossRef]
39. Li, L.G.; Feng, J.J.; Lu, Z.C.; Xie, H.Z.; Xiao, B.F.; Kwan, A.K.; Jiao, C.J. Effects of aggregate bulking and film thicknesses on water permeability and strength of pervious concrete. *Powder Technol.* **2022**, *396*, 743–753. [CrossRef]
40. Aminzadeh, M.; Kurfess, T. Automatic thresholding for defect detection by background histogram mode extents. *J. Manuf. Syst.* **2015**, *37*, 83–92. [CrossRef]
41. Soundrapandiyan, R.; Mouli, C.P. Adaptive Pedestrian Detection in Infrared Images Using Background Subtraction and Local Thresholding. *Procedia Comput. Sci.* **2015**, *58*, 706–713. [CrossRef]
42. Xie, F.; Bao, L.; Zheng, Y.; Chen, L.; Wang, R.; Li, G.; Cui, J. The mechanical properties, shrinkage mitigation, and bond performance of recycled powder based alkali-activated paste for surface enhancement of recycled concrete aggregate. *Constr. Build. Mater.* **2025**, *486*, 141993. [CrossRef]
43. Torres, A.; Hu, J.; Ramos, A. The effect of the cementitious paste thickness on the performance of pervious concrete. *Constr. Build. Mater.* **2015**, *95*, 850–859. [CrossRef]
44. Gomes, C.D.S.; Nguyen, D.Q.; Li, W. Shrinkage and carbonation of alkali-activated calcined clay-ground granulated blast furnace slag (GGBFS) concrete. *Cem. Concr. Res.* **2025**, *194*, 107899. [CrossRef]
45. Sha, F.; Zhang, S.M.; Sun, X.C.; Fan, G.X.; Diao, Y.; Duan, X.F.; Wang, H. Mechanical performance and pore characteristics of pervious concrete. *Case Stud. Constr. Mater.* **2024**, *21*, e03674. [CrossRef]
46. Yang, J.; Guo, Y.; Tam, V.W.; Tan, J.; Shen, A.; Zhang, J.; Zhang, C.; Lyu, Z. Research on pore-clogging behavior and mechanism in pervious concrete prepared with recycled aggregate. *Constr. Build. Mater.* **2023**, *384*, 131420. [CrossRef]
47. Wang, X.; Liu, Z.; Liu, C.; Wang, L.; Chen, M.; Yue, G. Study of mix design and performance of alkali-activated concrete with recycled concrete aggregate. *Constr. Build. Mater.* **2023**, *400*, 132882. [CrossRef]
48. Tejas, S.; Pasla, D. Approach to design sustainable alkali-activated slag recycled aggregate concrete, Mechanical and microstructural characterization. *Case Stud. Constr. Mater.* **2024**, *21*, e03886. [CrossRef]
49. Yap, P.S.; Chen, C.Z.P.; Goh, Y.; Ibrahim, H.A.; Mo, K.H.; Yuen, C.W. Characterization of pervious concrete with blended natural aggregate and recycled concrete aggregates. *J. Clean. Prod.* **2018**, *181*, 155–165. [CrossRef]
50. Song, H.; Fan, S.; Wan, K.; Yao, J.; Yin, W.; Lee, Y. Balancing mechanical and permeability properties of pervious concrete through inter-aggregate pore structure optimization. *J. Build. Eng.* **2025**, *106*, 112537. [CrossRef]

51. Sánchez-Mendieta, C.; Galán-Díaz, J.J.; Martinez-Lage, I. Relationships between density, porosity, compressive strength and permeability in porous concretes, Optimization of properties through control of the water-cement ratio and aggregate type. *J. Build. Eng.* **2024**, *97*, 110858. [CrossRef]
52. Shan, J.; Zhang, Y.; Wu, S.; Lin, Z.; Li, L.; Wu, Q. Pore characteristics of pervious concrete and their influence on permeability attributes. *Constr. Build. Mater.* **2022**, *327*, 126874. [CrossRef]
53. Yu, F.; Sun, D.; Hu, M.; Wang, J. Study on the pores characteristics and permeability simulation of pervious concrete based on 2D/3D CT images. *Constr. Build. Mater.* **2019**, *200*, 687–702. [CrossRef]
54. Gao, Q.; Li, X.G.; Shi, X.D.; Li, X.L.; Lyu, X.J.; Zhu, X.N.; Ren, Y.G. Clean and high-value recycling approach for waste concrete powder, Mechano-chemical activation of pozzolanic activity. *Powder Technol.* **2025**, *458*, 120988. [CrossRef]
55. Zhou, Z.; Yang, Z.; Cheng, S.; Yang, L. Effect of recycled concrete powder on the performance of alkali-activated slag. *Case Stud. Constr. Mater.* **2025**, *22*, e04811. [CrossRef]
56. Taha, A.; Alnahhal, W. Synergistic effects of recycled concrete powder, GGBFS, and basalt fibers on mechanical and durability performance of recycled aggregate concrete. *Structures* **2025**, *71*, 108058. [CrossRef]
57. Su, C.; Zhang, J.; Ding, Y. Research on reactivity evaluation and micro-mechanism of various solid waste powders for alkali-activated cementitious materials. *Constr. Build. Mater.* **2024**, *411*, 1134374. [CrossRef]

Disclaimer/Publisher's Note: The statements, opinions and data contained in all publications are solely those of the individual author(s) and contributor(s) and not of MDPI and/or the editor(s). MDPI and/or the editor(s) disclaim responsibility for any injury to people or property resulting from any ideas, methods, instructions or products referred to in the content.